Journal of Organometallic Chemistry 881 (2019) 130–138

Contents lists available at ScienceDirect

Journal of Organometallic Chemistry

journal homepage: www.elsevier.com/locate/jorganchem

Synthesis and characterization of tetracarbonylmolybdenum(0) and pentacarbonyltungsten(0) complexes of TADDOL-derived, monodentate P-donor ligands

Ethan C. Cagle, Gary M. Gray*

University of Alabama at Birmingham, Department of Chemistry, Birmingham, AL, USA

ARTICLE INFO

Article history:
Received 15 October 2018
Received in revised form
9 November 2018
Accepted 12 November 2018
Available online 4 December 2018

ABSTRACT

TADDOL-derived P-donor ligands are of interest as ligands in transition metal catalyzed transformations; however, few studies have been conducted on the steric and electronic properties of P-donor ligands derived from TADDOL. To gain more insight into these properties four tetracarbonylmolybdenum(0) and two pentacarbonyltungsten(0) complexes of monodentate P-donor ligands derived from TADDOL have been studied. These studies show that exchanging the chloro substituent on the phosphorus for OMe increases the donor ability of the ligand and that the *cis*-tetracarbonylmolybdenum(0) complex of the ligand having the OMe substituent spontaneously isomerizes in solution. X-ray crystallographic analyses indicate that the orientations of the 1,3,2-dioxaphosphepane ring and the aryl substituents are not always conserved, even within the same complex.

1. Introduction

Since the original reports of the synthesis of TADDOLs by Seebach and coworkers [1], substituted TADDOLs have become important precursors to chiral organic molecules and chiral ligands in transition metal catalysts [2–5]. The interest in the use of TADDOLs is due to multiple factors: 1) TADDOL can easily be synthesized from the readily available chiral tartaric acid; 2) multiple P-donor ligands (phosphochlorodite esters, phosphites, phosphoramidites and phosphonites) can easily be synthesized from the diol; 3) many derivatives of the TADDOL can easily be achieved by modifying the aryl substituents or the acetal ring (Fig. 1) [5].

Despite the successes of TADDOL-derived P-donor ligands in catalytic transformations, the coordination chemistry of these ligands in transition metal complexes has not been extensively studied. This is particularly true for TADDOL-derived phosphite ligands. As of this writing, the structure of only one coordination compound with a TADDOL-derived phosphite has been determined [4].

To better understand how TADDOL-derived phosphite ligands behave when coordinated to transition metals in catalytic systems, the coordination geometries and electronic properties of simple, monodentate phosphite ligands should be studied. In this paper, we present the syntheses, and the NMR spectroscopic and X-ray crystallographic characterizations of *cis*- and *trans*-$Mo(CO)_4$ complexes with two TADDOL-derived monodentate P-donor ligands. The electronic properties of the ligands were determined by measuring their $|^1J_{WP}|$ coupling constants in their $W(CO)_5$ complexes. A Rh(I) complex of the monodentate TADDOL-derived phosphite ligand was also evaluated as a catalyst for the hydroformylation of styrene to provide a baseline for future comparisons with catalysts having more complicated TADDOL-derived phosphites.

2. Results and discussion

2.1. Ligand synthesis and NMR characterization

The TADDOL-derived phosphochloridite ester (**L1**) was synthesized by a previously published literature protocol [6]. Scheme 1 shows the reaction pathway for the conversion of **L1** into the monodentate TADDOL-derived phosphite ligand **L2.** The reagents and products involved in these reactions are highly air-sensitive; therefore, Schlenk techniques were used.

The $^{31}P\{^1H\}$ NMR spectrum of **L2** displayed a singlet at 133.78 ppm that is shifted upfield relative to the $^{31}P\{^1H\}$ NMR

* Corresponding author.
E-mail address: gmgray@uab.edu (G.M. Gray).

https://doi.org/10.1016/j.jorganchem.2018.11.018
0022-328X/

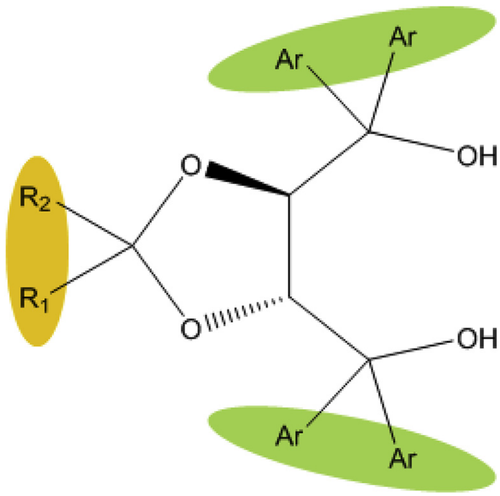

Fig. 1. Areas of modification to achieve various TADDOL-derived P-donor ligands.

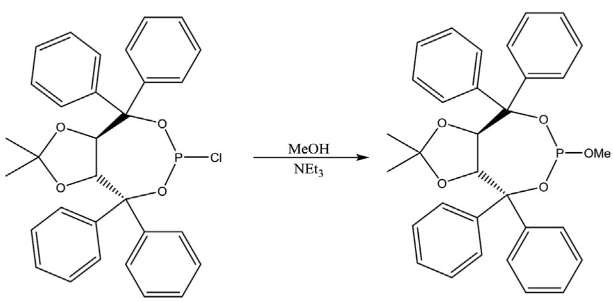

Scheme 1. Synthesis of **L2**.

resonance of **L1** (148.92 ppm). One peak is expected as the RR chirality of the starting dimethyl 2,3-O-isopropylidene-L-tartrate is neither lost in the formation of TADDOL nor in the formation of the P-donor ligands. The ^{1}H NMR spectrum of **L2** displays four distinct regions. The aromatic region shows a complex second-order resonance due to the multiple couplings within the aromatic rings between chemically and magnetically inequivalent protons. The C-H protons in the acetal ring give rise to two broad doublets. This splitting pattern appears to be due to coupling to the other acetal proton, which is magnetically inequivalent, as well as long range coupling to the phosphorus. The -$POCH_3$ protons give rise to two separate doublets. This could be due to loss of the C_2 symmetry because of the pyramidal phosphorus and conformational equilibrium between different arrangements about the 1,3,2-dioxaphosphepane. Finally, the furthest upfield resonances are singlets due to the methyl substituents on the acetal ring.

L1 and **L2** hydrolyze when exposed to air, therefore $^{31}P\{^{1}H\}$ and ^{1}H NMR spectra were used to evaluate their purity. After the purity was determined, the ligands were used to synthesize coordination complexes with tetracarbonylmolybdenum(0) and pentacarbonyltungsten(0) metal centers. Additionally, **L2** was used in the Rh(I) catalyzed hydroformylation of styrene.

2.2. Styrene hydroformylation catalyzed by the Rh(I) complex of L2

Rhodium(I) complexes containing **L2** were used as catalysts in the hydroformylation of styrene (Scheme 2). The results for these reactions are given in Table 1 and are compared to those obtained with an analogous P-donor ligand 2,2'-($C_{12}H_8O_2$)$POCH_3$, **L3**. Two

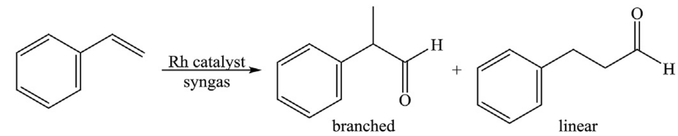

Scheme 2. Rh(I) catalyzed hydroformylation of styrene.

Table 1
Results of Styrene Hydroformylation Catalyzed by Rh(I) complexes of **L2** or **L3**.[a]

	Ligand				
	None[b]		L2		L3 [10]
Temperature (°C)	45	80 [10]	45	80	80
iso-selectivity (%)	81 (82)	47 (47)	89 (89)	77 (78)	86 (86)
ee (%)	–	–	7 (6) [R]	3 (3) [R]	–
k x 10^4 (s^{-1})	0.1 (0.1)	0.76 (0.88)	0.3 (0.1)	2.9 (2.9)	8.3 (8.2)
Completion (%)	100 (100)	100 (100)	100 (91)	100 (100)	100 (100)

[a] Results for duplicate experiments are shown in parentheses. Conditions (all ratios are molar): solvent = dichloromethane, CO/H2 = 1:1, P = 20 atm, substrate/Rh = 1000:1, ligand/Rh = 2.4:1. The pseudo-first-order rate constant, k, was obtained from a first-order fit of pressure drop versus time using Graphical Analysis software. ^{1}H NMR was used to determine % iso after a pressure change was no longer observed. No hydrogenation was observed. GC/MS was used to determine *ee*.
[b] The only pro-catalytic species present is $Rh(CO)_2(acac)$.

catalytic runs were performed at each set of conditions in order to measure reproducibility. The activities and regioselectivities were also measured under the same conditions in the absence of any P-donor ligand to determine the effects of the ligands.

Because the active catalyst forms *in situ*, the catalytically active species is not known. Possibilities include $RhH(CO)_{2+n}(phosphite)_{2-n}$ (n = 1, 0), $HRh(CO)_n$ (n = 3,4), and rhodium carbonyl clusters depending on the reactions conditions [7–9]. Martin and co-workers showed that increasing the P-donor ligand concentration has no effect on the regioselectivity of the reaction but drastically decreases the activity. This suggests that the active catalyst is formed at low ratios of ligand to rhodium [10].

Catalytic runs at 80 °C and 20 atm of syn gas with **L2** present in solution show increases in both *iso*-selectivity and activity when compared to those with only $Rh(CO)_2(acac)$ but show decreases in both *iso*-selectivity and activity when compared to catalytic runs with the biphenol-derived P-donor ligand (**L3**) in solution. These and previously reported results [10] suggest that the lower steric hindrance around the P-donor atom in **L3** leads to a higher *iso*-selectivity and a more active catalyst under this set of reaction conditions. The catalytic runs with **L2** present in solution showed a slight enantiomeric excess (3%) of the R enantiomer of the *iso* product.

It is well established that decreasing the temperature in the hydroformylation of styrene results in higher *iso*-selectivites and lower rates [11]. With this in mind, catalytic runs were conducted with **L2** in solution at 45 °C. While the catalyst with **L2** showed an *iso*-selectivity near 90%, a marked improvement over catalytic solutions containing only $Rh(CO)_2(acac)$ at the same temperature, the reaction took more than 20 h to reach completion. At the lower temperatures, the enantiomeric excess increased slightly from 3% R to 7% R.

2.3. Model complexes

2.3.1. Use in studies of coordination geometries

During alkene hydroformylation, catalysts with Rh(I) metal centers exhibit numerous coordination geometries. Because of this, it is beneficial to study ligands used in such reactions in a variety of chemical environments that model the coordinate geometries observed in these reactions. In addition, it is also possible to use coupling of NMR-active metal nuclei to phosphorus to evaluate the effect of substituents on the donor ability of the ligand [12–18] and the σ-character of the W-P bond [12,19].

2.4. Synthesis and characterization of molybdenum model complexes

The *cis*-$Mo(CO)_4(L)_2$ (L = **L1**, **L2**) complexes were synthesized using the synthetic pathway shown in Scheme 3 with dry DCM as the solvent. These reactions took no more than 2 h. Following each reaction, the mixture was evaporated to dryness, and the norbornadiene byproduct was removed though diffusion recrystallization using DCM/methanol. Some spontaneous *cis*/*trans* isomerization occurred during the purification of **2a**.

To determine the *trans*:*cis* equilibrium ratios for each complex, solid mercury(II) chloride was added to solutions of the complexes in THF-d^8. The $^{31}P\{^1H\}$ NMR spectra were then obtained for each sample at regular intervals until an equilibrium had been established. Upon addition of the $HgCl_2$, **2a** immediately and completely transformed to *trans*-$Mo(CO)_4$(**L2**)$_2$ (**2b**). The isomerization of **1a** to *trans*-$Mo(CO)_4$(**L1**)$_2$ (**1b**), whose $^{31}P\{^1H\}$ NMR spectra are shown in Fig. 2, took 5.25 h; reaching equilibrium at a 4:1 ratio of **1b** to **1a**. These reaction mixtures were then filtered through silica gel to obtain pure **1b** and **2b**.

The complexes (**1a**-**2b**) were characterized by $^{31}P\{^1H\}$, $^{13}C\{^1H\}$, and ^1H NMR spectroscopy. The $^{31}P\{^1H\}$ NMR spectral data for all complexes in this study are summarized in Table 2. All the resonances of the molybdenum complexes are singlets. That of **1a** showed an upfield shift of 5 ppm from that of **L1**, while that of **2a** showed a downfield shift of nearly 26 ppm from that of **L2**. The very different coordination chemical shifts could be due to different conformational changes about the phosphorus upon coordination to the Mo(0) center. The resonances of the trans complexes, **1b** and **2b**, are downfield of resonances of the respective *cis* complexes, **1a** and **2a**, with that of **2a** exhibiting a much larger coordination chemical shift. It is somewhat surprising that exchanging a chloro substituent for a methoxy substituent would have such a large effect on the coordination chemical shifts.

The $^{13}C\{^1H\}$ NMR spectra of **1a** and **2a** display the multiplets common for *cis* and *trans* metal carbonyls between 206 and 213 ppm. In both cases, the resonances of carbonyls *cis* to both P-donor ligands are upfield of those for carbonyls *trans* to one of the P-donor ligands. The $^{13}C\{^1H\}$ NMR spectra of **1b** and **2b** only display the multiplets for carbonyls *cis* to both P-donor ligands.

The ^1H NMR spectra for **1a**-**2b** each show a downfield set of three doublets and an upfield complex multiplet for the aromatic protons. The upfield multiplet exhibits splitting that seems to be influenced by both by the coordination geometries of the P-donor ligands and the nature of third substituent on the phosphorus. Two doublets upfield of the aromatic proton resonances are due to the two protons of the acetal ring. The chemical shifts of these doublets are also sensitive to both the coordination geometry of the $Mo(CO)_4$ center and the nature of third substituent on the phosphorus. Lastly, the protons for the acetal methyls give rise to two singlets whose chemical shifts show the same sensitivity to the coordination geometry of the $Mo(CO)_4$ center and the nature of third substituent on the phosphorus as do those of the resonances the acetal ring protons.

2.5. Synthesis and characterization of tungsten model complexes

The $W(CO)_5L$ complexes (**1c**, **2c**) were synthesized as shown in Scheme 4 using dry THF as the solvent. These reactions required up to 48 h to reach completion.

Complexes **1c** and **2c** were characterized by $^{31}P\{^1H\}$, $^{13}C\{^1H\}$, and ^1H NMR spectroscopy. The $^{31}P\{^1H\}$ NMR spectra of the tungsten complexes **1c** and **2c** each displays a singlet with a superimposed doublet due to the ^{185}W isotope (I = ½). While the resonances of both complexes are upfield of those of their respective free ligands, the resonance of **1c** shows a great upfield shift than does that of **2c**.

The $^{13}C\{^1H\}$ NMR spectra of **1c** and **2c** show doublets for the carbonyls *cis* to both P-donor ligands and for the carbonyl *trans* to the P-donor ligands. These doublets also have satellite peaks due to the $|^1J_{WC}|$ coupling between the carbonyl carbons and the ^{185}W isotope.

The ^1H NMR spectra of **1c** and **2c** are similar to those of **1a** and **2b**; however, the splitting patterns are less complex in **1c** and **2c** presumably due to the presence of only one P-donor ligand.

The magnitudes of the $|^1J_{WP}|$ coupling constants allow the relative donor abilities of the P-donor ligands to be determined [12–18]. Based on the coupling constants in Table 2, replacing the chloro group in **L1** with the OMe group in **L2** increases the donor ability of the ligand. Likewise, the σ-character of the **L1**-W bond is slightly greater than is the σ-character of the **L2**-W bond.

2.6. X-ray crystal structures of model complexes

X-ray quality crystals of most of the metal complexes synthesized in this research were obtained. The details of the individual data collections are in Table S1. In each case, the X-ray data confirmed the coordination geometry and agreed with NMR spectroscopic analyses. Select bond lengths and angles are given in Tables 3–4 and the structural diagrams are shown in Figs. 3–7. All the structures were solved without issue.

Each of the molybdenum carbonyl complexes has a distorted octahedral metal center. The largest distortion from the ideal angle is in the P-Mo-P bonds in **1a** and **2a** (99.29(5)° and 103.20(5)°, respectively) and in the C-Mo-P angles for the carbonyl ligands *cis*

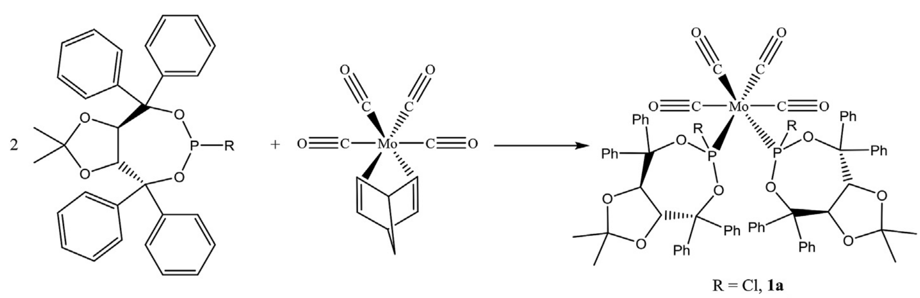

Scheme 3. Synthesis of **1a** and **2a**.

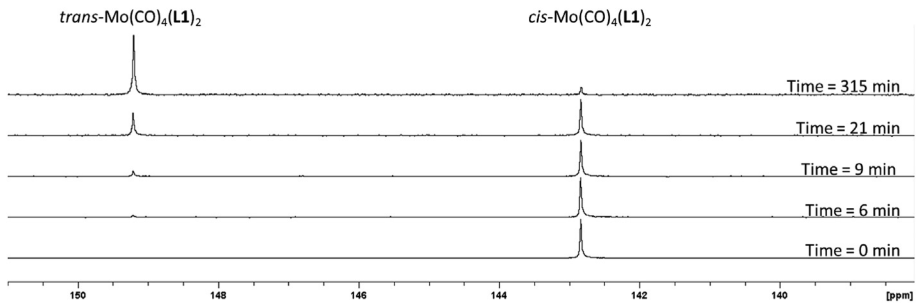

Fig. 2. *cis*/*trans* isomerization reaction of **1a** to **1b** with catalytic $HgCl_2$.

Table 2
^{31}P NMR chemical shifts of synthesized compounds.

Ligand	Free Ligand	*cis*-$Mo(CO)_4(L)_2$	*trans*-$Mo(CO)_4(L)_2$	$W(CO)_5(L)$
L1	148.92 (s)	143.08 (s)	149.2 (s)	110.89 (s), 110.89 (d, $\lvert ^1J_{WP}\rvert = 432.5$ Hz)
L2	133.78 (s)	159.54 (s)	168.18 (s)	132.89 (s), 132.91 (d, $\lvert ^1J_{WP}\rvert = 403.3$ Hz)

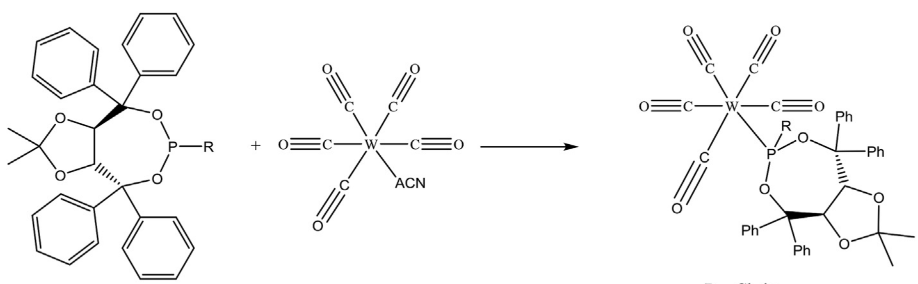

R = Cl, **1c**
= OMe, **2c**

Scheme 4. Synthesis of **1c** and **2c**.

Table 3
Select bond distances of metal (1a-2 b M = Mo, 1c M = W) complexes (Å).

(Å)	1a	1b	2a	2b	1c
C-M [*trans*-CO to P-donor]	2.01(1)	–	2.01(1)	–	2.018(5)
C-M [*cis*-CO to P-donor]	2.05(1)	2.05(1)	2.04(1)	2.04(1)	2.05(1)
C-O [*trans*-CO to P-donor]	1.14(1)	–	1.13(1)	–	1.126(7)
C-O [*cis*-CO to P-donor]	1.13(1)	1.13(1)	1.13(1)	1.13(1)	1.13(2)
M-P	2.443(1)	2.394(1)	2.458(1)	2.404(1)	2.430(1)

Table 4
Select bond angles (°) of molybdenum complexes.

(°)	1a	1b	2a	2b	1c
P1-Mo-P2	99.29(5)	176.73(2)	103.20(5)	179.48(4)	–
C(1)-Mo-P1	172.2(2)	90.42(8)	171.0(2)	91.5(1)	176.3(1)
C(1)-Mo-P2	86.7(2)	91.96(8)	85.4(2)	88.9(1)	–
C(2)-Mo-P1	87.3(2)	90.81(7)	84.7(2)	87.5(2)	89.8(1)
C(2)-Mo-P2	172.8(2)	87.09(7)	170.9(2)	92.2(2)	–
C(3)-Mo-P1	86.1(2)	88.46(7)	85.5(2)	90.5(1)	90.2(2)
C(3)-Mo-P2	91.6(2)	89.19(7)	90.5(2)	89.1(1)	–
C(4)-Mo-P1	94.2(2)	93.05(7)	88.8(2)	91.4(2)	90.6(2)
C(4)-Mo-P2	86.9(2)	89.24(7)	88.9(2)	88.9(2)	–
C(5)-Mo-P1	–	–	–	–	87.4(1)

to both of the P-donor ligands, which deviate significantly from the ideal 90°. None of the structures exhibited significantly different C-O bond lengths for carbonyls *cis* to both the P-donor ligands and those *trans* to one of the P-donor ligands as might be expected due to the different orbital overlap [20,21]. With exception for **1b**, the

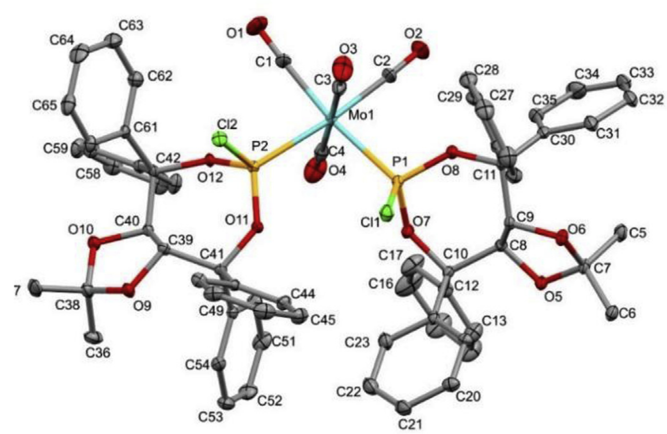

Fig. 3. Solid-state structure of **1a**, Thermal ellipsoids are drawn at the 30% probability level, hydrogen atoms and solvent are omitted for clarity.

Mo-P bond lengths are also within the average determined by Mogul 2.440(17) [22].

It is of interest to determine if each of the P-donor ligands exhibits a similar conformation within each complex and between the complexes. The most basic aspect of the ligand conformation is the conformation of the 1,3,2-dioxaphosphepane ring. Fig. 8 shows that the seven torsion angles around the 1,3,2-dioxaphosphepane ring have similar orientations and the angles, with the exception of one

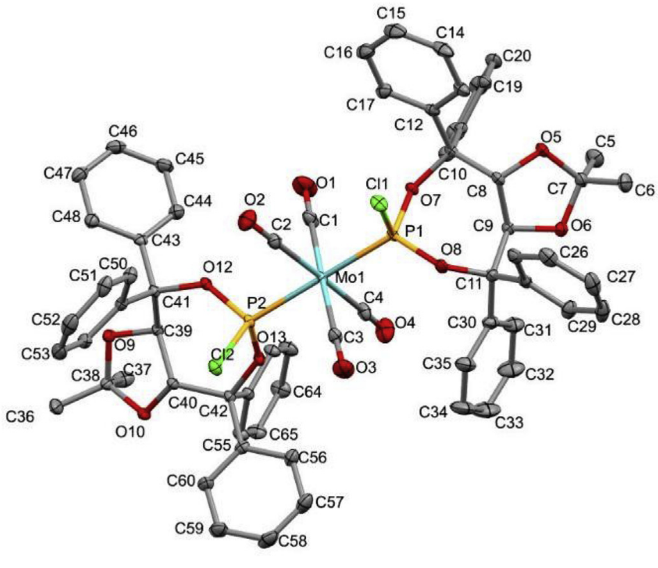

Fig. 4. Solid-state structure of **1b**, Thermal ellipsoids are drawn at the 30% probability level, hydrogen atoms are omitted for clarity.

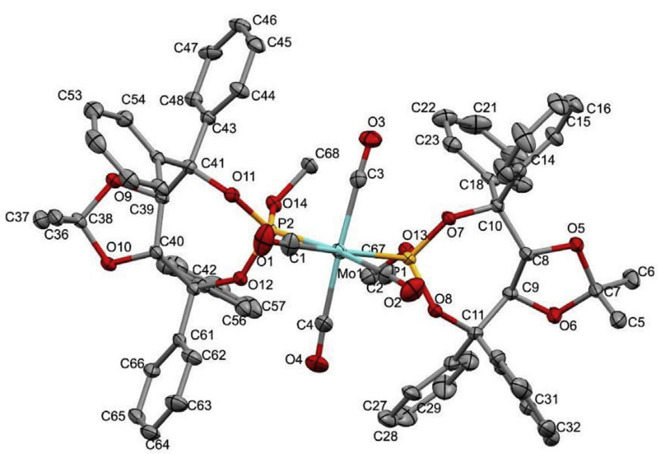

Fig. 5. Solid-state structure of **2a**, Thermal ellipsoids are drawn at the 30% probability level, hydrogen atoms and solvent are omitted for clarity.

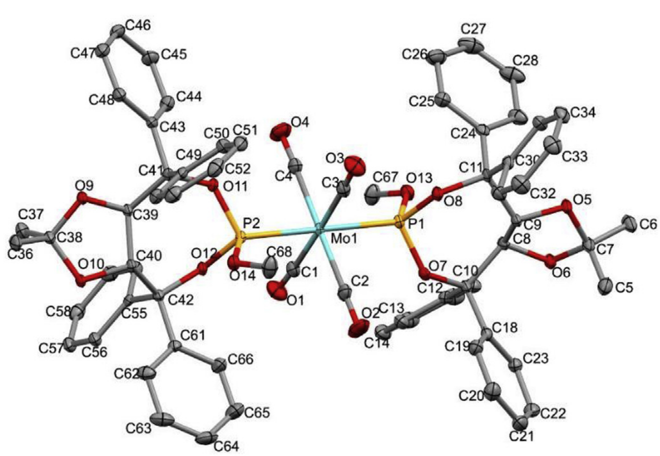

Fig. 6. Solid-state structure of **2b**, Thermal ellipsoids are drawn at the 30% probability level, hydrogen atoms and solvent are omitted for clarity.

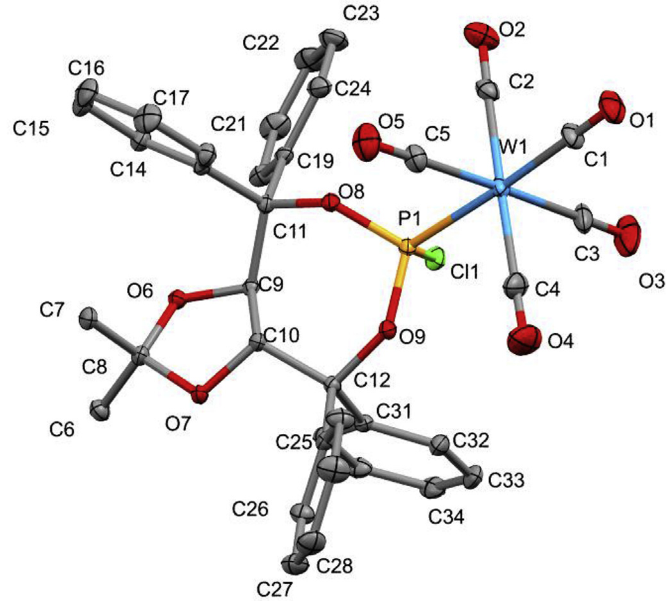

Fig. 7. Solid-state structure of **1c**, Thermal ellipsoids are drawn at the 30% probability level, hydrogen atoms and solvent are omitted for clarity.

ligand in **1b**, and that these torsion angles fall within a range of about 20°. In the conserved conformation, the oxygen and non-bridgehead carbons are planar or nearly planar. The phosphorus atom is above this plane while the bridgehead carbons are twisted about this plane. This twist is due to the chirality of the starting alcohol and can also be seen in the structure of the previously synthesized *trans*-$PdCl_2$ complex of a polyether derived TADDOL ligand [4]. In the unique conformation (P1 of **2a**), the ligand exhibits a more symmetrical orientation with a pseudo-C_2 rotation axis through the phosphorus and the quaternary carbon in the acetal ring. It is interesting to note that the preferred conformation of the 1,3,2-dioxaphosphepane ring is found in the structure of **1c**, which is a pentacarbonyltungsten(0) complex that contains only a single P-donor ligand that should experience minimal intramolecular steric interactions.

A related aspect of the ligand conformation is the orientation of the phenyl rings relative to the 1,3,2-dioxaphosphepane rings. These are determined by the torsion angles about the bonds between the *ipso*-phenyl carbons and the 1,3,2-dioxaphosphepane rings. The torsion angles reported in Table 5 are calculated using the adjacent 1,3,2-dioxaphosphepane ring oxygen and the *ortho*-phenyl carbon that gives the smaller torsion angle. The torsions in **1a** and **2a** are equal in sign and similar in magnitude. This could be expected as the ligands in the *cis* complexes are held in close proximity. However, in the *trans* complexes and in the pentacarbonyltungsten(0) complex, the torsion angles of the aryl rings are not conserved. This suggests that fewer orientations are possible when the ligands are adjacent to one another.

A comparison of the conformations of the 1,3,2-dioxaphosphepane rings and aryl groups in the TADDOL-derived P-donor ligands in the same $Mo(CO)_4$ complexes is given by the wireframe overlays of the ligands in Fig. 9. These overlays indicate that the conformations of the ligands are most conserved in **2a**. The conformations of the ligands are also quite similar in **2b**, but the methoxy and molybdenum exchange positions on the phosphorus. The greatest differences in the ligand conformations are seen in **1b** in which the different 1,3,2-dioxaphosphepane ring conformations result in very different aryl ring conformations.

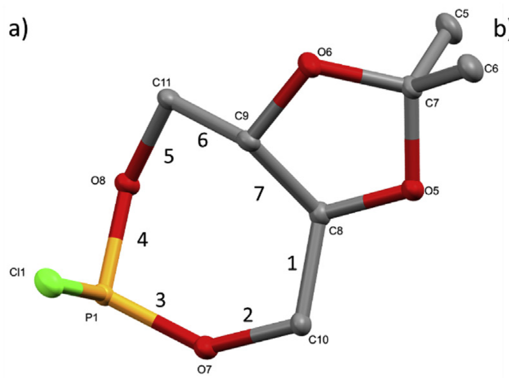

b)

bond	1a P1	1a P2	2a P1	2a P2	1b P1	1b P2	2b P1	2b P2	1c P1
1	65.2(6)	62.8(6)	69.2(6)	70.6(5)	47.1(2)	66.8(2)	67.6(4)	67.2(4)	72.3(4)
2	-36.9(7)	-55.2(6)	-54.1(6)	-45.5(6)	29.9(3)	-51.7(2)	-56.1(4)	-54.5(5)	-46.6(4)
3	43.1(5)	60.7(5)	60.8(5)	51.4(5)	-28.3(2)	56.6(2)	66.8(4)	67.1(4)	50.7(3)
4	-69.0(5)	-51.2(5)	-68.4(5)	-72.3(4)	-46.9(2)	-62.9(2)	-73.8(4)	-81.8(4)	-72.4(3)
5	35.9(7)	7.6(7)	30.1(7)	38.9(6)	41.8(2)	24.6(3)	31.7(5)	38.5(5)	39.1(4)
6	48.0(6)	60.9(6)	48.7(6)	43.3(6)	43.9(2)	51.9(2)	46.3(4)	43.0(4)	42.5(4)
7	-100.5(6)	-93.8(6)	-97.0(6)	-98.8(5)	-103.5(2)	-95.5(2)	-92.4(4)	-90.3(4)	-98.5(4)

Fig. 8. a) Ligand from **1a** with 1,3,2-dioxaphosphepane torsion angles numbered. b) the 1,3,2-dioxaphosphepane torsion angles for all complexes.

Table 5
Torsion angles (°) to the aryl rings in the molybdenum complexes (O-C_q-C_{ipso}-C_{ortho}).

(°)	1a	2a	1b	2b	1c
Ar 1	58.1	41.49	34.86	−30.96	−42.9(5)
Ar 2	4.2	25.07	39.45	−46.13	−15.9(5)
Ar 3	−44.33	−46.17	−38.19	−46.46	26.8(5)
Ar 4	−22.34	−25.01	−18.45	−19.71	44.9(5)
Ar 5	46.28	42.84	−23.15	−19.93	–
Ar 6	38.61	33.51	−24.38	38.1	–
Ar 7	−59.94	−50.3	22.5	−40.51	–
Ar 8	−24.53	−23.06	47.24	−21.19	–

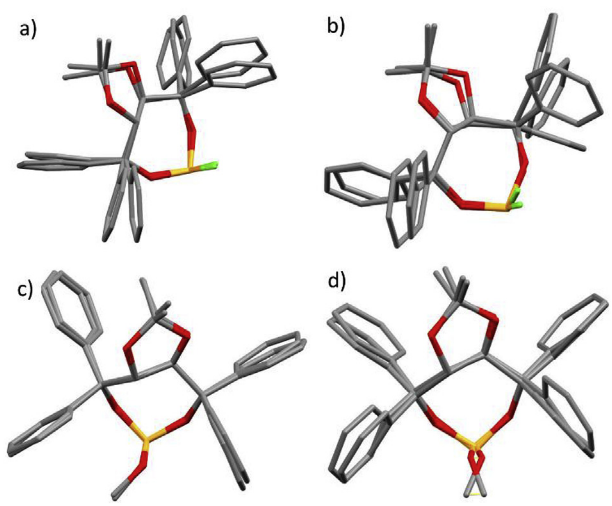

Fig. 9. a) wireframe overlay of both ligands of **1a**. b) wireframe overlay of both ligands of **1b**. c) wireframe overlay of both ligands of **2a**. d) wireframe overlay of both ligands of **2b**.

The fact that the ligand conformations are more similar in the *cis* complexes suggests that a requirement for ligands designed to yield high enantioselectivities in the hydroformylation of styrene would be backbones that hold the TADDOL-derived P-donor groups in close proximity and restrict the conformational mobility of the 1,3,2-dioxaphosphepane rings and their aryl substituents. This approach is seen in the TADDOL-derived P-donor ligands with *o*-catechol-derived backbones reported by Breit and coworkers [3g].

To determine how the arrangement of the aryl rings affect the steric bulk of the phosphorus donor ligands, cone angles (θ), were determined for each ligand (Table 6) [23–25]. The complex with the smallest difference in cone angles is **2a** (2.4°), which is expected given the similarities in the conformations of the two ligands. The other complexes have cone angles that differ by 10–15° with all the cone angles falling within a 20° range.

Table 6
Cone angles, θ, (°) about the Mo-Px bond of the molybdenum complexes.

(°)	1a	1b	1c	2a	2b
P1	154.6	154.4	147.8	151.7	135.5
P2	140.4	141.8	–	154.1	145.5

3. Conclusion

The first family of TADDOL-derived P-donor ligands coordinated to $(CO)_4Mo(0)$ centers have been prepared and have been characterized by $^{31}P\{^1H\}$, $^{13}C\{^1H\}$, and ^1H NMR spectroscopies and by X-ray crystallography. These results show that the orientation of the 7-membered 1,3,2-dioxaphosphepane ring is conserved in all but one of the nine ligands coordinated to Mo(0) centers. The ability of these ligands to exhibit different conformations could affect the chirality transfer in catalysis to prochiral substrates. This suggests that better chirality transfer could potentially be seen in ligands that have less conformational flexibility, like bidentate bridging ligands. Also, the spontaneous cis/trans isomerization of **2a** to **2b** was observed. An equilibrium ratio of 4:1 (**1b**:**1a**) was observed when $HgCl_2$ was added to solution containing **1a**.

A Rh(I) complex of **L2** was evaluated as a catalyst for the HF of styrene. This ligand showed improved activity and regioselectivity over solutions that contained no ligand under all reaction conditions tested. At 45 °C, these complexes showed an *iso*-selectivity of nearly 90%; however, the lower temperature resulted in a diminished catalytic activity. The enantioselectivity of the reaction increased as the temperature was lowered, but never rose above a 7% ee of the R enantiomer. Backbones that lead to less conformational variability may lead to better chirality transfer and therefore higher enantioselectivities.

Complexes with TADDOL-derived P-donor ligands coordinated to $(CO)_5W(0)$ centers have been prepared and have been characterized by $^{31}P\{^1H\}$, $^{13}C\{^1H\}$, and ^1H NMR spectroscopies and X-ray crystallography. The magnitudes of the $|^1J_{WP}|$ coupling constants in these complexes are useful in determining the relative donor abilities of the P-donor ligands and demonstrate that **L1** is a better donor than **L2**.

This study is the first to date that probes the coordination of TADDOL-derived phosphite ligands to octahedral metal centers. Octahedral geometries are often observed in transition metal catalyzed reactions. Due to this, it would be of continued interest to study bidentate TADDOL-derived phosphite ligands coordinated to similar metal centers.

4. Experimental

4.1. Materials and methods

Tetrahydrofuran (THF) was initially dried over $MgSO_4$ for at least 12 h, then distilled from CaH_2 and finally distilled from Na/benzophenone. It was stored over molecular sieves (3 Å; 8–12 mesh) and used within a few hours. Toluene was dried by distillation from Na and stored over molecular sieves (3 Å; 8–12 mesh). Dichloromethane (DCM) was dried by distillation from CaH_2 and stored over molecular sieves (3 Å; 8–12 mesh). Triethylamine was initially dried over KOH for a minimum of 12 h, distilled from Na/benzophenone, and stored over molecular sieves (3 Å; 8–12 mesh). Other solvents were reagent grade and were degassed using high-purity (99.998%) nitrogen before use. Literature procedures were used to prepare *cis*-$Mo(CO)_4(nbd)$ (nbd = norbornadiene) [26], $W(CO)_5(ACN)$ [27] (ACN = acetonitrile), $Rh(CO)_2(acac)$ (acac = acetylacenoate) [28], and **L1** [6].

4.2. Characterization

NMR spectra were recorded on Bruker DRX-400, Avance-500, and Avance-700 MHz spectrometers. Solutions of the complexes in deuterated solvents were prepared under a stream of N_2 gas, and all NMR experiments were performed at room temperature. The $^{31}P\{^1H\}$ NMR spectra were referenced to external 85% H_3PO_4 in a coaxial tube that also contained $CDCl_3$, and the $^{13}C\{^1H\}$ and ^1H NMR spectra were referenced to internal $SiMe_4$ (TMS). Some assignments were based on 2D NMR spectra (^1H–^{13}C HSQC, ^1H - ^1H COSY). Elemental analyses (C and H) were performed by Atlantic Microlabs, Inc.

$C_{31}H_{28}O_4POCH_3$ (**L2**). A solution of 0.66 g (1.2 mmol) of **L1** in 25.0 mL of dry THF was added dropwise to a stirred solution of 0.050 mL (1.2 mmol) methanol and 0.17 mL (1.2 mmol) of dry triethylamine in 25 mL of dry THF. After addition was completed, the dropping funnel was washed with 10.0 mL of dry THF, and the reaction mixture was then stirred for 2 h at room temperature under a constant stream of $N_2(g)$. The solution was then cannula transferred to a dry 200 mL fritted funnel containing a mixture of Celite and basic alumina and filtered via positive N_2 pressure into a 100 mL Schlenk flask to remove the triethylammonium chloride precipitate byproduct and any hydrolysis byproducts. The residue in the filter was next washed with two 10 mL portions of dry THF. Removal of the solvent from the filtrate through rotary evaporation and vacuum drying yielded 0.57 g (88%) of spectroscopically pure **L2** as a colorless solid. $^{31}P\{^1H\}$ NMR (chloroform-*d*): δ 133.78 (s).^1H NMR (chloroform-*d*): δ 7.55–7.51 (m, 4H, Ar-CH), 7.46–7.45 (m, 2H, Ar-CH), 7.36–7.14 (m, 14H, Ar-CH), 5.07 (bd, 1H, $|^3J_{HH}| = 8$ Hz, TADDOL-CH), 5.02 (bd, 1H, $|^3J_{HH}| = 8$ Hz, TADDOL-CH), 3.48 (d, 1.5H, $|^2J_{HP}| = 10$ Hz, $POCH_3$), 3.47 (d, 1.5H, $|^2J_{HP}| = 10$ Hz, $POCH_3$), 0.91 (s, 3H, CCH_3), 0.42 (s, 3H, CCH_3).

cis-$Mo(CO)_4(C_{31}H_{28}O_4PCl)_2$ (**1a**). A solution of 0.40 g (0.75 mmol) of **L1** and 0.10 g (0.37 mmol) *cis*-$Mo(CO)_4(nbd)$ in 25.0 mL dry THF was stirred at room temperature under a nitrogen atmosphere for 2 h. Then, the THF was removed by rotary evaporation to yield a brown solid. The solid product was triturated with 15.0 mL methanol and dried *in vacuo* overnight to yield crude **1a** as an off-white powder. Recrystallization from DCM/methanol yielded 0.22 g (47%) of analytically pure **1a** in the form of colorless crystals. Anal. Calc for $C_{66}H_{56}O_{12}P_2MoCl_2\cdot 0.3\ CH_2Cl_2$: C, 61.57; H, 4.40. Found: C, 61.52; H, 4.65. $^{31}P\{^1H\}$ NMR (chloroform-*d*): δ 143.08 (s). ^1H NMR (chloroform-*d*): δ 7.58 (d, $|^3J_{HH}| = 8$ Hz, 2H, Ar-CH), 7.56 (d$|^3J_{HH}| = 8$ Hz, 2H, Ar-CH), 7.38 (d, $|^3J_{HH}| = 8$ Hz, 2H, Ar-CH), 7.34 (bs, 2H, Ar-CH), 7.28–7.09 (m, 12H, Ar-CH), 5.94 (d, $|^3J_{HH}| = 8$ Hz, 1H, TADDOL-CH), 4.97 (d, $|^3J_{HH}| = 8$ Hz, 1H, TADDOL-CH), 1.29 (s, 3H, CH_3), 0.22 (s, 3H, CH_3). $^{13}C\{^1H\}$ NMR (chloroform-*d*): δ 211.77 (m, *trans*-CO), 205.90 (t, $|^2J_{CP}| = 15$ Hz, *cis*-CO), 144.79 (bs, TADDOL-C_q), 144.37 (s, Ar-C_q), 139.89 (bs, TADDOL-C_q), 139.40 (s, Ar-C_q), 129.18 (bs, Ar-CH), 129.03 (s, Ar-CH), 128.17 (s, Ar-CH), 127.89 (s, Ar-CH), 127.85 (s, Ar-CH), 127.81 (s, Ar-CH), 127.79 (s, Ar-CH), 127.77 (s, Ar-CH), 127.52 (s, Ar-CH), 127.44 (s, Ar-CH), 127.28 (s, Ar-CH), 127.04 (s, Ar-CH), 112.82 (s, $\underline{C}(CH_3)_2$), 81.84 (s, TADDOL-CH), 79.19 (s, TADDOL-CH), 27.64 (s, CH_3), 25.23 (s, CH_3).

cis-$Mo(CO)_4(C_{31}H_{28}O_4POCH_3)_2$ (**2a**). Using the procedure for **1a,** 0.57 g (1.1 mmol) of **L2** and 0.16 g (0.55 mmol) of $Mo(CO)_4(nbd)$ yielded 0.23 g (32%) of analytically pure **2a**. Calcd for $C_{68}H_{62}O_{14}P_2Mo\cdot 0.5\ CH_2Cl_2$: C, 63.28; H, 4.86. Found: C, 63.09; H, 5.09. $^{31}P\{^1H\}$ NMR (chloroform-*d*): δ 159.54 (s). δ 7.52 (d, $|^3J_{HH}| = 7$ Hz, 2H, Ar-H), 7.44 (d, $|^3J_{HH}| = 8$ Hz, 2H, Ar-H), 7.34 (d, $|^3J_{HH}| = 7$ Hz, 2H, Ar-H), 7.29 (bs, 2H, Ar-H), 7.20–7.11 (m, 10H, Ar-H), 7.08–7.05 (m, 3H, Ar-H), 5.83 (dd, $|^3J_{HH}| = 9$ Hz, $|^4J_{PH}| = 2$ Hz, 1H, TADDOL-CH), 4.73 (dd, $|^3J_{HH}| = 9$ Hz, $|^4J_{PH}| = 2$ Hz, 1H, TADDOL-CH), 1.94–1.93 (m, 3H, $POC\underline{H}_3$), 1.31 (s, 3H, CCH_3), 0.11 (s, 3H, CCH_3). $^{13}C\{^1H\}$ NMR (chloroform-*d*): δ 212.81 (m, *trans*-CO), 208.02 (t, $|^2J_{CP}| = 14$ Hz, *cis*-CO), 146.13 (s, Ar-C_q), 146.00 (bs, TADDOL-C_q), 142.23 (s, Ar-C_q), 140.90 (bs, TADDOL-C_q), 129.63 (s, Ar-CH), 128.76 (s, Ar-CH), 127.87 (s, Ar-CH), 127.52 (s, Ar-CH), 127.47 (s, Ar-CH), 127.44 (s, Ar-CH), 127.39 (s, Ar-CH), 127.39 (s, Ar-CH), 127.31 (s, Ar-CH), 127.18 (s, Ar-CH), 127.15 (s, Ar-CH), 111.83 (s, $\underline{C}(CH_3)_2$), 82.06 (s, TADDOL-CH), 78.54 (s, TADDOL-CH), 52.09 (bs, $PO\underline{C}H_3$), 27.91 (s, CH_3), 25.24 (s, CH_3).

trans-$Mo(CO)_4(C_{31}H_{28}O_4PCl)_2$ (**1b**). A few crystals of $HgCl_2$ were added to a stirred solution of 0.068 g (0.13 mmol) of **1a** in 20 mL of THF. The reaction was followed by $^{31}P\{^1H\}$ NMR spectroscopy and, when an equilibrium between **1a** and **1b** had been established after 5.25 h, the solution was filtered through silica gel. The THF was removed by from the filtrate by rotary evaporation to yield crude **1b** as an off-white powder. Recrystallization from DCM/methanol yielded 0.021 g (31%) of spectroscopically pure **1b** as colorless crystals. $^{31}P\{^1H\}$ NMR (chloroform-*d*): δ 149.20 (s). ^1H NMR (chloroform-*d*): δ 7.64 (d, $|^3J_{HH}| = 7$ Hz, 2H, Ar-H), 7.58 (d, $|^3J_{HH}| = 7$ Hz, 2H, Ar-H), 7.38 (d, $|^3J_{HH}| = 7$ Hz, 2H, Ar-H), 7.31–7.28 (m, 7H, Ar-H), 7.26–7.24 (m, 5H, Ar-H), 7.20–7.19 (m, 2H, Ar-H), 5.87 (dd, $|^3J_{HH}| = 8$ Hz, $|^4J_{PH}| = 2$ Hz, 1H, TADDOL-CH), 4.94 (dd, $|^3J_{HH}| = 8$ Hz, $|^4J_{PH}| = 2$ Hz, 1H, TADDOL-CH), 1.21 (s, 3H, CCH_3), 0.22 (s, 3H, CCH_3). $^{13}C\{^1H\}$ NMR (chloroform-*d*): δ 205.76 (t, $|^2J_{PC}| = 13$ Hz), *cis*-CO), 144.64 (m, TADDOL-C_q), 144.29 (s, Ar-C_q), 140.22 (m, TADDOL-C_q), 139.74 (s, Ar-C_q), 128.81 (s, Ar-CH), 128.23 (s, Ar-CH), 127.94 (t, $|^4J_{CP}| = 5$ Hz, Ar-CH), 127.77 (s, Ar-CH), 127.73 (s, Ar-CH), 127.45 (s, Ar-CH), 127.24 (s, Ar-CH), 127.13 (s, Ar-CH), 112.95 (s, $\underline{C}(CH_3)_2$), 81.69 (s, 1H, TADDOL-CH), 79.09 (s, 1H, TADDOL-CH), 27.56 (s, CH_3), 25.41 (s, CH_3).

trans-$Mo(CO)_4(C_{31}H_{28}O_4POCH_3)_2$ (**2b**). Using the procedure for **1b,** 0.050 g (0.0.037 mmol) of **2a** yielded 0.040 g (81%) of spectroscopically pure **2b**. $^{31}P\{^1H\}$ NMR (chloroform-*d*): δ 168.18 (s) .^1H NMR (chloroform-*d*): δ 7.79 (d, $|^3J_{HH}| = 8$ Hz, 2H, Ar-H), 7.65 (d, $|^3J_{HH}| = 8$ Hz, 2H, Ar-H), 7.45–7.43 (m, 4H, Ar-H), 7.35–7.17 (m, 12H, Ar-H), 5.87 (dd, $|^3J_{HH}| = 9$ Hz, $|^4J_{PH}| = 2$ Hz, 1H, TADDOL-CH), 4.83 (dd, $|^3J_{HH}| = 9$ Hz, $|^4J_{PH}| = 2$ Hz, 1H, TADDOL-CH), 2.54–2.53 (m, 3H, OCH_3), 1.45 (s, 3H, CCH_3), 0.18 (s, 3H, CCH_3). $^{13}C\{^1H\}$ NMR (chloroform-*d*): δ 208.06 (t, $|^2J_{PC}| = 13$ Hz), *cis*-CO), 146.99 (s, TADDOL C_q), 145.87 (s, Ar-C_q), 142.48 (s, TADDOL-C_q), 141.11 (s, Ar-C_q), 129.37 (bs, Ar-CH), 128.27 (s, Ar-CH), 128.05 (s, Ar-CH), 127.51 (s, Ar-CH), 127.37 (s, Ar-CH), 127.32 (s, Ar-CH), 127.29 (s, Ar-CH), 127.22 (s, Ar-CH), 127.20 (s, Ar-CH), 127.13 (s, Ar-CH), 126.87 (s, Ar-CH), 111.63 (s, $C(CH_3)_2$), 82.69 (s, TADDOL-CH), 79.88 (s, TADDOL-CH), 52.52 (s, OCH_3), 27.89 (s, $C\underline{C}H_3$), 24.89 (s, $C\underline{C}H_3$).

$W(CO)_5(C_{31}H_{28}O_4PCl)$ (**1c**). Solid $W(CO)_5(ACN)$ (0.16 g, 0.42 mmol)) was added to a stirred solution of 0.22 g (0.42 mmol) of **L1** in 50.0 mL of dry THF. After 48 h, the solution was decanted and filtered through a 2 cm pad of neutral alumina. THF was removed from the filtrate by rotary evaporation to yield crude **1c** as a yellow powder. Recrystallization from DCM/hexanes yielded 0.36 g (98%) of analytically pure **1c** as a yellow powder. Anal. Calcd for ($C_{36}H_{28}ClO_9PW$ + 1.1 DCM): C, 47.72; H, 3.22. Found: C, 47.71; H, 3.59. $^{31}P\{^1H\}$ NMR (chloroform-*d*): δ 110.89 (s), 110.89 (d, $|^1J_{WP}| = 433$ Hz) .^1H NMR (chloroform-*d*): δ 7.66 (d, $|^2J_{HH}| = 8$, 2H, Ar-H), 7.62 (d, $|^2J_{HH}| = 8$, 2H, Ar-H), 7.44 (d, $|^2J_{HH}| = 8$, 2H, Ar-H), 7.38–7.28 (m, 14H, Ar-H), 5.91 (d, $|^2J_{PH}| = 8$, 1H, TADDOL-CH), 5.08 (d, $|^2J_{PH}| = 8$, 1H, TADDOL-CH), 1.24 (s, 3H, CH_3), 0.32 (s, 3H, CH_3). $^{13}C\{^1H\}$ NMR (chloroform-*d*): δ 198.44 (d, $|^2J_{PC}| = 54$ Hz, *trans*-CO), 198.44 (dd, $|^2J_{PC}| = 54$ Hz, $|^1J_{WC}| = 142$ Hz *trans*-CO), 195.09 (d, $|^2J_{PC}| = 11$ Hz, *cis*-CO), 195.09 (dd, $|^2J_{PC}| = 11$ Hz, $|^1J_{WC}| = 127$ Hz *cis*-CO), 144.01 (d, $|^2J_{PC}| = 7$ Hz, TADDOL-C_q), 143.68 (s, Ar-C_q), 139.66 (d, $|^2J_{PC}| = 7$ Hz, TADDOL-C_q), 139.20 (s, Ar-C_q), 128.80 (s, Ar-CH), 128.42 (s, Ar-CH), 128.16 (s, Ar-CH), 127.87 (s, Ar-CH), 127.61 (s, Ar-CH), 127.18 (s, Ar-CH), 127.10 (s, Ar-CH), 113.51 (s, $\underline{C}(CH_3)_2$), 81.47 (d, TADDOL-CH, $|^2J_{PC}| = 4$ Hz), 79.00 (d, TADDOL-$\underline{C}$H, $|^2J_{PC}| = 6$ Hz), 30.38 (s, CH_3), 25.50 (s, CH_3).

$W(CO)_5(C_{31}H_{28}O_4POCH_3)$ (**2c**). Using the procedure for **1c**, 0.22 g (0.43 mmol) of **L2** and 0.10 g (0.43 mmol) of $W(CO)_5(ACN)$ yielded 0.17 g (93%) of analytically pure **2c**. Anal. Calc for ($C_{37}H_{31}O_{10}PW$): C, 52.25; H, 3.67. Found: C, 52.28; H, 3.61. $^{31}P\{^1H\}$ NMR (chloroform-*d*): δ 132.91 (d, $|^1J_{WP}| = 403$ Hz), 132.90 (s) .^1H NMR (chloroform-*d*): δ 7.68 (d, $|^3J_{HH}| = 8$ Hz, 2H, Ar-H), 7.59 (d, $|^3J_{HH}| = 8$ Hz, 2H, Ar-H), 7.43–7.20 (m, 16H, Ar-H), 5.80 (d, $|^3J_{HH}| = 8$ Hz, 1H, TADDOL-CH), 4.88 (d, $|^3J_{HH}| = 8$ Hz, 1H, TADDOL-CH), 2.53 (d, $|^3J_{PH}| = 13$ HZ, 3H, $POCH_3$), 1.35 (s, 3H, CCH_3), 0.22 (s, 3H, CCH_3). $^{13}C\{^1H\}$ NMR (chloroform-*d*): δ 198.30 (d, $|^2J_{PC}| = 41$ Hz, *trans*-CO), 198.30 (dd, $|^2J_{PC}| = 41$ Hz, $|^1J_{WC}| = 140$ Hz *trans*-CO), 195.55 (d, $|^2J_{PC}| = 11$ Hz, *cis*-CO), 195.55 (dd, $|^2J_{PC}| = 11$ Hz, $|^1J_{WC}| = 126$ Hz *cis*-CO), 146.08 (s, Ar-C_q), 145.01 (d, $|^2J_{PC}| = 8$ Hz, TADDOL-C_q), 142.62 (s, Ar-C_q), 142.07 (s, Ar-C_q), 141.53 (s, Ar-C_q), 140.31 (d, $|^2J_{PC}| = 7$ Hz, TADDOL-C_q), 128.36 (s, Ar-CH), 128.27 (s, Ar-CH), 127.86 (s, Ar-CH), 127.77 (s, Ar-CH), 127.69 (s, Ar-CH), 127.65 (s, Ar-CH), 127.59 (s, Ar-CH), 127.45 (s, Ar-CH), 127.37 (s, Ar-CH), 127.19 (s, Ar-CH), 127.17 (s, Ar-CH), 127.15 (s, Ar-CH), 127.02 (s, Ar-CH), 126.90 (s, Ar-CH), 126.75 (s, Ar-CH), 112.39 (s, $\underline{C}(CH_3)_2$), 82.15 (d, $|^3J_{PC}| = 4$ Hz, TADDOL-CH), 79.33 (d, $|^3J_{PC}| = 4$ Hz, TADDOL-CH), 53.44 (d, $|^3J_{PC}| = 4$ Hz, OCH_3), 27.72 (s, $C\underline{C}H_3$), 25.11 (s, $C\underline{C}H_3$).

4.3. Hydroformylation of styrene

The hydroformylation reactions were carried out using a Parr Series 4560 minireactor connected to a high-pressure gas burette that introduced gas to the reactor at a constant pressure. The digitized reactor temperature, burette temperature, and burette pressure were monitored using Agilent Benchlink Data Logger software on a PC connected to an Agilent data acquisition switch unit. In a typical run, 9.0 mg (0.035 mmol) of $Rh(CO)_2(acac)$ and the appropriate amount of alkali metal salt, if used, were weighed and added to a 50 mL Schlenk round bottom flask which was then sealed, evacuated, and filled with N_2. To this flask was added the appropriate amounts of dry DCM and a stock solution containing a known concentration of the appropriate ligand dissolved in dry DCM so that the mole ratio of ligand:rhodium was 2.4:1 and the total volume was 22 mL. This solution was then added to the reactor via cannula transfer under positive N_2 pressure through the substrate inlet valve. The reactor was then purged three times with a 1:1 H_2:CO (syngas) mixture, and then pressurized to 20 atm with syngas and heated to 80 °C with mechanical stirring. The reactor was maintained under these conditions for 45 min to allow for pre-catalyst equilibration and was then cooled to ~38 °C before pressure was slowly vented. Approximately 4.0 mL (35 mmol) of styrene was then injected into the reactor through the substrate inlet valve, after which the reactor was again pressurized to 20 atm with syngas and re-heated to 80 °C with mechanical stirring.

The progress of the reaction was monitored using the Agilent software. The activity of the catalyst was expressed in terms of a pseudo-first order rate constant (k). The pressure drop versus time data was fit to the natural exponential equation $P = (P_d)e^{-kt} + P_f$, where P_d is the pressure drop ($P_f - P_i$), P_f is the final pressure, and k (s^{-1}) is the pseudo-first order rate constant, using Graphical Analysis version 3.4 [29]. The regioselectivities (% *iso*) were determined from integrations of the ^1H NMR spectra of the reaction mixtures at the ends of the reactions. Enantioselectivities were measured using a chiral Supelco β-DEX 225 column and a Shimadzu GC/MS-QP5000 Spectrometer following the method developed by Whiteker and Klosin [30].

4.4. X-ray data collection and solution

A suitable single crystal was mounted on a MicroLoop (MiTeGen, Inc.) after coating in Paratone-N oil (Hampton Research Corp.). Data were collected at the specified temperature with a Bruker CCD diffractometer (SMART APEX2) fitted with a low temperature device (Oxford Cryostream). The diffractometer used graphite monochromated Cu Kα (λ = 1.54178 Å) radiation with a detector distance of 5 cm. The program SAINT was used to collect and reduce the data [31]. Unit cell constants are based upon the refinement of the XYZ-centroids found using a standard indexing routine (APEX2) [32]. All data were corrected for Lorentz and polarization effects, and were scaled using the numerical method SADABS [33]. The structure was solved and refined using the Bruker SHELXTL Software Package [34]. Heavy atoms were found using either Direct Methods or Pattersons, and the remainder of the non-hydrogen atoms were located in difference Fourier maps. Full-matrix least-squares refinement on F^2 was performed on positional and anisotropic parameters for these atoms. Hydrogen atoms were placed in calculated positions with the appropriate molecular geometry δ (C-H = 0.96 Å). The isotropic thermal parameter associated with each hydrogen atom was fixed equal to 1.2 times the U_{eq} of the atom to which it is bound. CCDC 1871695 (**1a**), 1871696 (**1b**), 1871697 (**2a**), 1871698 (**2b**), 1877439 (**1c**) contains the supplementary crystallographic data for this paper. The data can be obtained free of charge from The Cambridge Crystallographic Data Center via www.ccdc.cam.ac.uk/structures.

Acknowledgements

The authors acknowledge the National Science Foundation for support under grant DPS-1158862. E.C. wishes gratefully thanks NSF Alabama EPSCoR for funding under a Graduate Research Scholars (GRSP) graduate fellowship.

Appendix A. Supplementary data

Supplementary data to this article can be found online at https://doi.org/10.1016/j.jorganchem.2018.11.018.

References

[1] D. Seebach, A.K. Beck, R. Imwinkelried, S. Roggo, A. Wonnacott, Helv. Chim. Acta 70 (1987) 954–974.
[2] (a) D. Seebach, A.K. Beck, A. Heckel, Angew. Chem. Int. Ed. 40 (2001) 92–138; (b) H. Pellissier, Tetrahedron 64 (2008) 10279–10317.
[3] (a) A. Falk, L. Fiebig, J.-M. Neudorfl, A. Adler, H.-G. Schmalz, Adv. Synth. Catal. 353 (2011) 3357–3362;

(b) Q. Naeemi, M. Dindaroglu, D.P. Kranz, J. Velder, H.-G. Schmalz, Eur. J. Org Chem. (2012) 1179–1185;
(c) S.A. Moteki, K. Toyama, Z. Liu, J. Ma, A.E. Holmes, J.M. Takacs, Chem. Commun. 48 (2012) 263–265;
(d) M. Drusan, W. Lolsberg, A. Skvorcova, H.-G. Schmalz, R. Sebesta, Eur. J. Org Chem. (2012) 6285–6290;
(e) A. Falk, A.-L. Goderz, H.-G. Schmalz, Angew. Chem. Int. Ed. 52 (2013) 1576–1580;
(f) C.S. Marques, M. Dindaroglu, H.-G. Schmalz, A.J. Burke, RSC Adv. 4 (2014) 6035–6041;
(g) S. Allmendinger, H. Kinuta, B. Breit, Adv. Synth. Catal. 357 (2015) 41–45;
(h) K. Kitamura, N. Shimada, C. Stewart, A.C. Atesin, T.A. Ates-in, M.A. Tius, Angew. Chem. Int. Ed. 54 (2015) 6288–6291.

[4] L. Rovira, H. Fernandez-Perez, A. Vidal-Ferran, Organometallics 35 (2016) 528–533.
[5] J. Pedroni, N. Cramer, Chem. Commun. 51 (2015) 17647–17657.
[6] R. Kranich, K. Eis, O. Geis, S. Muhle, J.W. Bats, H.G. Schmalz, Chem. Eur J. 6 (2000) 2874–2894.
[7] M. Garland, G. Bor, Inorg. Chem. 28 (1989) 410–413.
[8] M. Garland, P. Pino, Organometallics 10 (1991) 1693–1704.
[9] A. van Rooy, E.N. Orij, P.C.J. Kamer, P.W.N.M. van Leeuwen, Organometallics 14 (1995) 34–43.
[10] J.R. Martin, E.C. Cagle, A.L. Lucius, G.M. Gray, Organometallics 35 (2016) 2609–2620.
[11] A.T. Axtell, J. Klosin, G.T. Whiteker, Organometallics 28 (2009) 2993–2999.
[12] S.D. Hastings, H. Byrd, L.N. Gray, M.J. Jablonsky, J.L. Freeman, G.M. Gray, Eur. J. Inorg. Chem. 16 (2013) 2900–2911.
[13] W.H. Hersh, P. Xu, B. Wang, J.W. Yom, C.K. Simpson, Inorg. Chem. 35 (1996) 5453–5459.
[14] W.A. Schenk, W. Buchner, Inorg. Chim. Acta. 70 (1983) 189–196.
[15] T.J. Malosh, S.R. Wilson, J.R. Shapley, Inorg. Chim. Acta. 362 (2009) 2849–2855.
[16] R.L. Keiter, J.G. Verkade, Inorg. Chem. 8 (1969) 2115–2120.
[17] R.V. Honeychuck, W.H. Hersh, Inorg. Chem. 26 (1987) 1826–1828.
[18] C. Wallis, P.G. Edwards, M. Hanton, P.D. Newman, A. Stasch, C. Jones, R.P. Tooze, Dalton Trans. (2009) 2170–2177.
[19] G. Frenking, K. Wichmann, N. Fröhlich, J. Grobe, W. Golla, D.L. Van, B. Krebs, M. Läge, Organometallics 21 (2002) 2921–2930.
[20] H. Byrd, J.D. Harden, J.M. Butler, M.J. Jablonsky, G.M. Gray, Organometallics 22 (2003) 4198–4205.
[21] M.B. Murphy-Jolly, S.B. Owens Jr., J.L. Freeman, G.M. Gray, C.M. Lawson, D.P. Shelton, Eur. J. Inorg. Chem. 2010 (2010) 5263–5271.
[22] I.J. Bruno, J.C. Cole, M. Kessler, J. Luo, W.D. Motherwell, L.H. Purkis, B.R. Smith, R. Taylor, R.I. Cooper, S.E. Harris, A.G. Orpen, J. Chem. Inf. Comput. Sci. 44 (2004) 2133–2144.
[23] C.A. Tolman, Chem. Rev. 77 (1977) 313–348.
[24] T.E. Müller, D.M.P. Mingos, Trans. Met. Chem. 20 (1995) 533–539.
[25] J.A. Bilbrey, A.H. Kazez, J. Locklin, W.D. Allen, J. Comput. Chem. 34 (2013) 1189–1197.
[26] W. Ehrl, R. Rinck, H.J. Vahrenkamp, Organomet. Chem. 56 (1973) 285–293.
[27] W.H. Hersh, Inorg. Chem. 29 (1990) 713–722.
[28] Y.S. Varshavskii, T.G. Cherkasova, Zh. Obshch. Khim. 12 (1967) 1709.
[29] Graphical Analysis 3, 2014.
[30] C.J. Cobley, J. Klosin, C. Qin, G.T. Whiteker, Org. Lett. 6 (2004) 3277–3280.
[31] Bruker SAINT+, Version V8.34A, 2013.
[32] Bruker APEX2, Version 2013.10-0, 2013.
[33] Bruker SADABS, Version 2012/1, 2012.
[34] G.M. Sheldrick, SHELXTL, V. Bruker, Analytical X-ray, Systems Inc., Madison, 2001.